Performance Assessment Modeling of a Generic SNF/HLW Repository in Salt with Coupled Thermal-Hydrologic Effects – 15423

S. David Sevougian*, Geoff A. Freeze*, W. Payton Gardner*, Glenn E. Hammond*, Paul E. Mariner*, and Robert J. MacKinnon*
*Advanced Nuclear Energy Programs Group, sdsevou@sandia.gov
Sandia National Laboratories
P.O. Box 5800, M.S. 0747
Albuquerque, NM 87185

ABSTRACT

This paper describes advances in performance assessment modeling of deep geologic repositories facilitated by a massively parallel, high-performance computing (HPC) environment. Our new Generic Disposal System Analysis (GDSA) Framework utilizes the massively parallel PFLOTRAN multi-physics code to simulate repository performance in the presence of coupled thermal-hydrologic-chemical processes, linked to DAKOTA, an HPC uncertainty sampling and propagation code that provides nested parallelism for multi-realization performance assessment and sensitivity analysis. This enhanced performance assessment (PA) modeling capability is demonstrated with deterministic and probabilistic simulations of a generic repository for SNF and HLW in bedded salt host rock, by comparing repository performance between a case with heat-generating waste ("thermal" case) and a case without heat generation ("isothermal" case). The simulation results provide preliminary insights into the effect of multi-physics processes and thermal-hydrologic coupling on the long-term behavior of a reference-case salt repository.

INTRODUCTION

The U.S. Department of Energy Office of Nuclear Energy (DOE-NE), Office of Used Nuclear Fuel Disposition is conducting scientific research to enable disposal of spent nuclear fuel (SNF) and high-level radioactive waste (HLW) in a variety of geologic media and generic repository concepts, including mined disposal in salt, clay/shale, and granite formations, and deep borehole disposal in granite formations. An important goal of this research is the development of an enhanced performance assessment (PA) modeling capability that utilizes high-performance computing environments to simulate important systems-level, multi-physics phenomena and couplings associated with the potential behavior of the geologic repository. The application of an HPC-capable modeling/simulation framework for repository performance assessment allows multi-physics couplings to be represented directly, rather than through simplified abstractions. It also allows for complex representations of the source term, e.g., the explicit representation of many individual waste packages. The overall objectives of this enhanced performance assessment modeling capability, or Generic Disposal System Analysis (GDSA) Framework, are:

1) Evaluate potential SNF/HLW disposal concepts and sites in various host rock media
2) Help prioritize generic RD&D activities and, later, site-specific RD&D activities
3) Support safety case development during all phases of repository investigations

METHODOLOGY

The development of any geologic repository takes place over a period of years and, as the repository program evolves, the level of completeness and rigor in the associated safety case [1, 2, 3] becomes more robust with additional data from scientific investigations and design engineering activities (i.e., the *technical bases* for the disposal system). These technical bases, when combined with *safety evaluations*

to determine their potential impact on repository performance, form an iterative process wherein the safety evaluation from one development phase feeds the technical bases at the next phase (Fig. 1). The safety evaluation (e.g., post-closure performance assessment of the repository system) is the most important quantitative analysis activity for assisting with prioritization of future R&D activities and resolution of remaining issues and uncertainties. Therefore, there must be a high degree of confidence in the capabilities of the performance assessment (PA) modeling tool(s). This confidence is enhanced when important multi-physics process couplings can be directly incorporated into a probabilistic PA framework. This is facilitated when the PA software is designed to be run in a parallel architecture in a high-performance computing (HPC) environment, which in turn provides the following benefits, as a result of shorter computational times:

- Less reliance on assumptions, simplifications, and abstractions, which increases transparency and confidence with both the regulator and other stakeholders
- More realistic and comprehensive representation in the PA simulations of (1) features, events, and processes (FEPs), including more detailed spatial-temporal representation of geometry (e.g., 3-D spatial heterogeneity), and (2) parameter and model uncertainty, both aleatory and epistemic
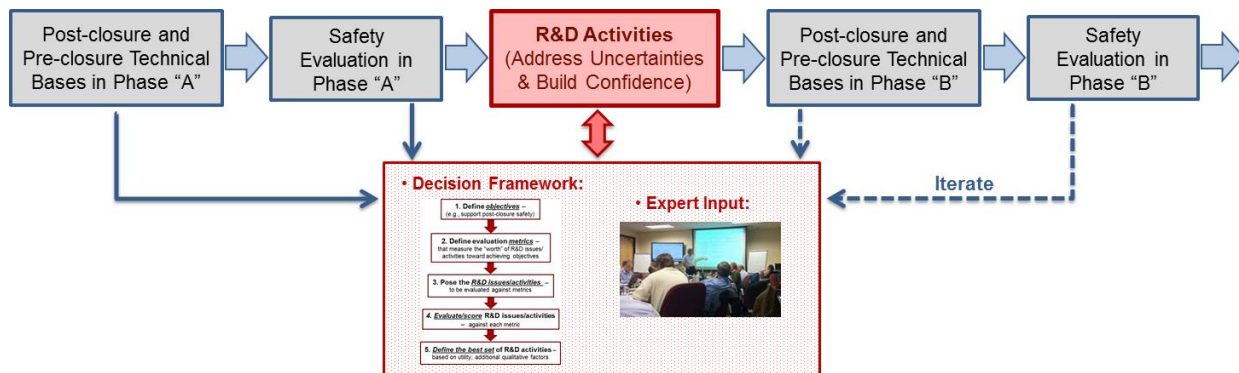

Fig. 1. Iteration of key elements of a repository safety case. {<u>Note</u>: Phases "A" and "B" are generic development phases such as "site characterization" or "licensing".}

The enhanced PA modeling capability supporting generic disposal system modeling includes two main components [4, Sec. 2]: (1) a *conceptual multi-physics model framework* and (2) a *computational framework*.

Conceptual Model Framework

The major steps in the development of the conceptual model include

- System Characterization – characterization of the regions and features of the disposal system, including property values and quantification of uncertainty
- System Design – specification of a disposal concept, repository, layout, and engineered design features
- FEPs and Scenario Analysis – identification and screening of potentially relevant FEPs and scenarios, for inclusion in scenario analysis and PA model(s) – see [2, Sec. 4.2] and [5]
- PA Model Construction – conceptual and mathematical representation of the FEPs and scenarios – e.g., see [6]

For a generic bedded salt repository the major features and processes of each of the regions are illustrated schematically in 1-D in Fig. 2. The features of the Engineered Barrier System (EBS) include the wastes (e.g., waste forms and cladding) and engineered features (e.g., waste package, buffer and/or backfill, and

seals/liner); the features of the Natural Barrier System (NBS) include the disturbed rock zone (DRZ), host rock, and other geological units (e.g., overlying or underlying aquifers); and the features of the Biosphere include the surface environment and receptor characteristics [7, 8]. The near field encompasses the EBS and the DRZ (i.e., the components influenced by the presence of the repository). The far field encompasses the remainder of the NBS (i.e., beyond the influence of the repository).
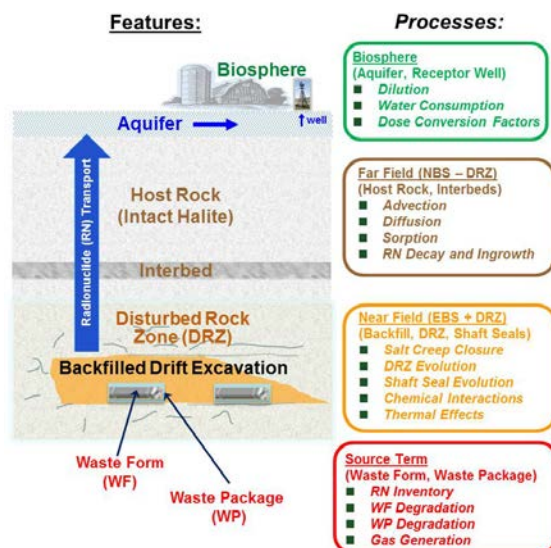

Fig. 2. Major FEP categories for a generic bedded salt repository.

Computational Framework

The most important software components of the PA computational framework are those associated with (1) uncertainty quantification, uncertainty propagation, and sensitivity analysis ("stochastic simulation") and (2) simulation of the multi-physics coupled processes ("domain simulation"), including spatial and temporal discretization, and numerical solution algorithms. As indicated in Fig. 3, the following open-source codes perform this core set of functions for the generic repository PA framework:

- DAKOTA – sensitivity analysis and uncertainty quantification [9]
- PFLOTRAN – multi-physics flow and reactive transport [10]

PFLOTRAN is an open source (https://bitbucket.org/pflotran/pflotran-dev), reactive multi-phase flow and transport simulator designed to leverage massively-parallel high-performance computing to simulate earth system processes. Parallelization is achieved through domain decomposition using the Portable Extensible Toolkit for Scientific Computation (PETSc) [11]. Sensitivity analysis and uncertainty quantification (UQ) for multi-realization PA analyses in an HPC environment are provided by DAKOTA (Design Analysis toolKit for Optimization and Terascale Applications).

As indicated in Fig. 3, there are three major elements of the PA domain simulation software:

- Source Term and EBS Evolution – A single code or a suite of codes to simulate coupled processes in the emplacement drifts and near-field, including heat generation from the inventory, waste form degradation, waste package degradation, coupled thermal-hydrologic-chemical-mechanical (THCM) effects, and radionuclide mobilization and transport.
- Far-Field Processes – This includes the simulation of multi-phase flow and solute transport, and other coupled THC processes, and is performed by PFLOTRAN.

- Biosphere Transport and Receptor Uptake – A biosphere code to represent the surface and biosphere processes contributing to the dose to a human receptor resulting from radionuclide releases from the NBS.

For the work presented here the latter two components are implemented in the PFLOTRAN code in a simplified fashion but more specialized software components will be coupled into the GDSA Framework in the future, e.g., an electrochemical "mixed potential model" for SNF degradation [12].
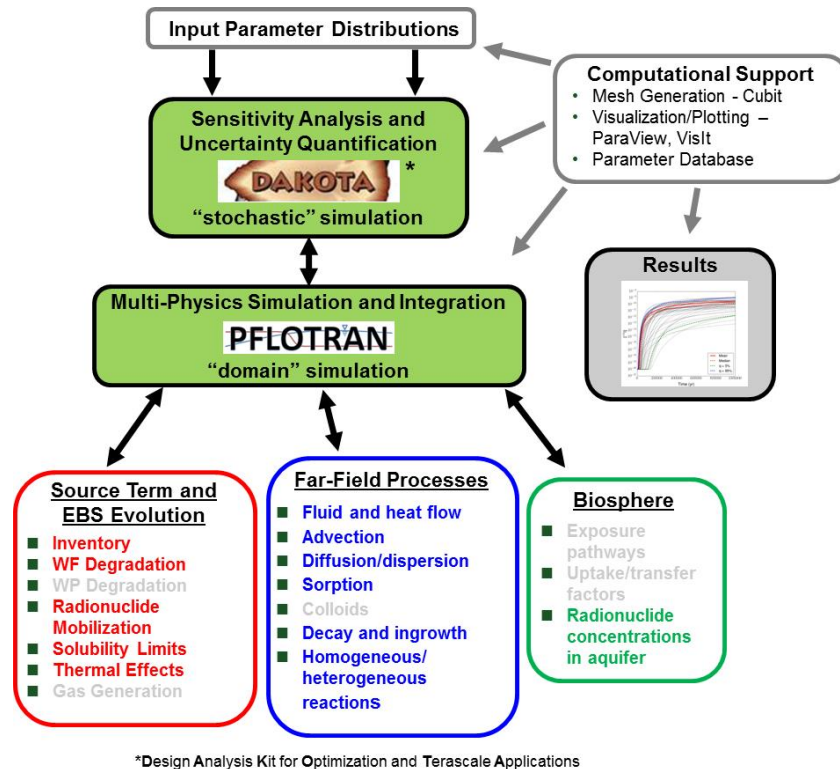

Fig. 3. High-level GDSA computational framework.

GENERIC SALT DISPOSAL MODEL AND REFERENCE CASE

Some of the capabilities of the GDSA Framework have been demonstrated previously by application to a model reference case for a generic repository in bedded salt [13, 14]. Certain modifications to the reference case are necessary to demonstrate the thermal-hydrologic capabilities of the framework, such as the addition of typical values for thermal conductivity in salt. Most of these updates are reported here but for a complete discussion of the entire model and reference case, see [15] and [13]. The initial focus of the generic reference cases remains the undisturbed scenario (e.g., performance in the absence of external events) rather than on disturbed scenarios (e.g., human intrusion, seismic activity). This is logical for generic repository analyses because disturbed scenarios are strongly dependent on site-specific information and regulatory considerations.

As described by Freeze et al. [13], the reference case inventory in the current version of the generic bedded salt reference case is limited to PWR SNF waste. There have been two important updates to the SNF waste form model: (1) a change in the fractional SNF waste form degradation rate and (2) a change to the instant release fraction of ^{129}I. Previously, the fractional SNF waste-form degradation rate was based on information from the Swedish repository program for degradation in chemically reducing granitic groundwaters [16]. However, more pertinent information from the German repository program

[17, Sec. 5.1.2.2] indicates that bromide concentrations found in brines typical of salt deposits (e.g., [18, App. SOTERM, TABLE SOTERM-2] will counteract the protective hydrogen effect in reducing waters, thereby making the SNF effectively "self-oxidizing" due to radiolysis. This results in SNF degradation rates typical of oxidizing EBS environments in other repository concepts, such as a repository in the unsaturated zone [19, TABLE 2.3.7-19]. TABLE I shows the new fractional degradation rate constants, λ, proposed for the salt reference case, where $m(t)/m_0 = e^{-\lambda t}$, with $m(t)$ being the mass of waste at any time t and m_0 being the initial mass.

TABLE I. SNF degradation rate constants, λ, in typical bromide-containing brines[a], used for the salt reference case.

Case	λ (s^{-1})	λ (d^{-1})	λ (yr^{-1})	Time for 50% Degradation (yrs)	Time for 95% Degradation (yrs)
Deterministic	1.1574×10^{-11}	10^{-6}	3.6525×10^{-4}	~ 1,900	~ 8,200
Probabilistic – Lower	1.1574×10^{-13}	10^{-8}	3.6525×10^{-6}	~ 190,000	~ 820,000
Probabilistic – Upper	1.1574×10^{-10}	10^{-5}	3.6525×10^{-3}	~ 190	~ 820

[a] from [17, Figs. 18 and 19]

PFLOTRAN does not currently have a fractional degradation rate option; so, as a surrogate, the SNF waste-form mineral is assigned a zeroth-order (linear) rate law that approximates the degradation times shown in TABLE I [15, Sec. 4.1]—giving complete dissolution in 7600 years.

Besides the radionuclide releases due to UO_2 matrix degradation, the release of some radionuclides from SNF includes a fast/instant fraction that is released upon waste package breach—predominantly from radionuclides located in the fuel and cladding gap and grain boundaries. The salt reference case described here assumed an instant release fraction of 11.25% for ^{129}I, based on the current inventory of light-water reactor SNF [20, TABLE 6.3.7-29]. A more comprehensive set of models and values for instant release fraction for PWR SNF at various burn-ups has been compiled by Sassani et al. [21, TABLE 3.2-1], with the Johnson 2005 model being recommended for high burn-up fuels, such as the 60 GWd/MT fuel being considered in the salt reference case. Using the Johnson 2005 model, a "best estimate" ^{129}I instant release fraction of 10% or a "pessimistic estimate" instant release fraction of 16% will be adopted in the future.

The salt reference case repository layout remains the same as Freeze et al. [13] and is based on a 200°C temperature constraint at the waste package surface. The salt reference case backfill remains the same as Freeze et al. [13], except that a value for tortuosity, τ, has been assigned and assumed to be given by $\tau = \phi^{1/3} = 0.48$, where ϕ is the total porosity. Tortuosity is necessary to properly represent the diffusion-dominant transport in salt repositories. All other media in the repository system have also been an assigned a tortuosity based on $\tau = \phi^{1/3}$ [22, 23], except for the host-rock halite, which is assumed to be given by $\tau = 0.01$, e.g., see [24, Sec. 7.4].

The thermal material properties for each material region, i.e., saturated thermal conductivity and specific heat capacity, are summarized in TABLE II. In addition, the reference-case domain (see Fig. 4) has an applied geothermal gradient in the vertical z-direction, based on a temperature of 20°C at the surface and 28°C at the bottom boundary over the total domain thickness of 945 m (thermal gradient thus equals 0.00847 °C/m). The simulated heat source (W/MTHM) represented by the decay of the radionuclides in 70,000 MTHM of 60 GWd/MT SNF was taken from Carter et al. [25], assuming 50 years of above-ground decay storage.

TABLE II. Key deterministic parameters for generic bedded salt reference case.

Model Region	Permeability (m^2)	Porosity	Tortuosity	Effective Diffusion Coefficient[a] (m^2/s)	Longitudinal Dispersivity (m)[f]	Saturated Thermal Conductivity[c] (W/m·°K)	Specific Heat Capacity[c] (J/kg·°K)	Grain Density[d] (kg/m^3)
Waste Package	1.00×10^{-13}	0.500	1.00	6.90×10^{-10}	0.5	16.7	466	5000.0
Backfill	1.00×10^{-18}	0.113	0.48	1.24×10^{-10}	0.2	2.5	927	2170.0
Shaft (sealed)	1.58×10^{-20}	0.113	0.48	1.24×10^{-10}	20.0	2.5	927	2170.0
DRZ	1.12×10^{-16}	0.0129	0.23	6.82×10^{-12}	1.0	4.9	927	2170.0
Halite	3.16×10^{-23}	0.0182	0.01	4.19×10^{-13}	50.0	4.9	927	2170.0
Interbed (anhydrite)	1.26×10^{-19}	0.011	0.22	5.57×10^{-12}	50.0	4.9	927	2960.0
Aquifer[c]	1.00×10^{-13}	0.150	0.53	1.83×10^{-10}	50.0	1.5	959	2820.0[e]
Sediments[b,e]	1.00×10^{-15}	0.20	0.58	2.67×10^{-10}	50.0	1.5	927	2700.0

[a] Effective diffusion coefficient = (free water diffusion coefficient) × (tortuosity) × (porosity)
[b] from [26, TABLES 2.2 and 2.4]
[c] [27, App. D]
[d] Crain's Petrophysical Handbook and PetroWiki (online)
[e] [28, TABLE 26 (Culebra dolomite)]
[f] Transverse dispersivity = 0

APPLICATION OF THE SALT DISPOSAL SYSTEM MODEL

This section describes new simulation results from the application of the GDSA framework to the generic salt repository reference case. In comparison to the isothermal simulations by Freeze et al. [13, 14], new simulations shown here represent a test of the GDSA framework for a heat-generating repository, in order to demonstrate coupled TH effects. Two cases are shown and compared: (1) an updated isothermal simulation over the full length of the domain in the *x*-direction and (2) a new thermal simulation over the same domain. The full-length domain in the direction of fluid flow and transport removes an unrealistic zero-gradient boundary condition for diffusive transport at the former "symmetry" boundary in the middle of the repository, which was used as the upstream boundary condition by Freeze et al. [14]. It is also extends the domain 1000 meters down-gradient of the withdrawal well, to eliminate any boundary effects near the well. This implies that the new domain reported on here is 12,642 m, as opposed to the 5809-m domain in Freeze et al. [14].

As described by Freeze et al. [14], the 70,000 MTHM of PWR SNF is assumed to be distributed throughout 84 pairs of emplacement drifts (168 total drifts), where each drift is 809 m long and contains 80 waste packages of 12-PWR SNF with a 10-m center-to-center spacing between waste packages that are 5 m in length. The current GDSA simulation domain for the salt reference case models a single drift pair containing 160 waste packages, i.e., it is a three-dimensional "slice" of the full model domain, as indicated by the gray shading in Fig. 4. The resulting 3-D model domain is 12,642 m long (464 grid cells) in the *x*-direction, 20 m wide (5 grid cells) in the *y*-direction, and 945 m high (92 grid cells) in the *z*-direction. The model domain and regions shown in Fig. 4 are reproduced in Fig. 5 at a scale and orientation consistent with the model results, i.e., directly from the PFLOTRAN simulation grid. Also, shown in Fig. 5 is a not-to-scale enlargement of 8 out of the 160 waste packages in a single drift pair. The biosphere receptor location is assumed to be located at the ground surface directly above the withdrawal well, at a distance of 5,000 m laterally from the downgradient edge of the emplacement drifts.

Deterministic Isothermal Simulation Results

The salt repository *isothermal* simulations were run using the PFLOTRAN "Richards" option, whose governing equations are documented by Lichtner et al. [29]. The fluid velocity magnitude (m/yr) and vector fields in all regions of the simulation domain (resulting from the applied hydraulic gradient of 0.0013) are shown in Figs. 6 and 7. Figure 6 shows Darcy velocity magnitude at 10 years for essentially the full domain, while Fig. 7 shows velocity vectors and magnitude at 1000 years for a portion of the domain closer to the repository region. For this isothermal case, the velocity magnitude and direction remains essentially constant for the entire 1,000,000-year simulation time, which may be contrasted with the convection cells that develop in the thermal simulation discussed below. [Note: The small green "dashes" in these plots represent the velocity in the thin anhydrite interbeds adjacent to the upper and lower boundaries of the repository zone.]
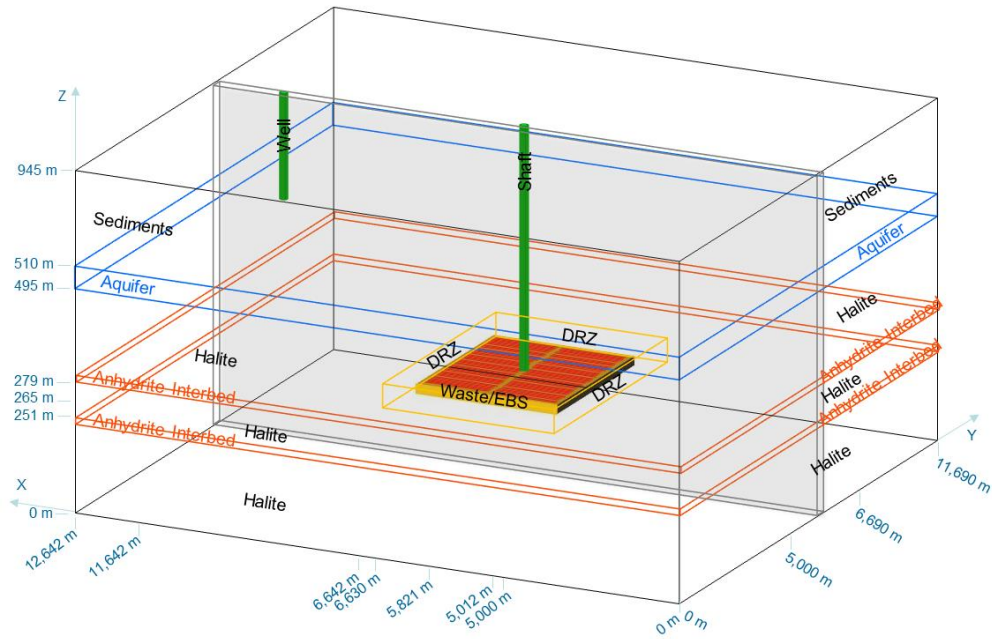

Fig. 4. GDSA simulation domain (gray shading) for the salt reference case (not to scale).
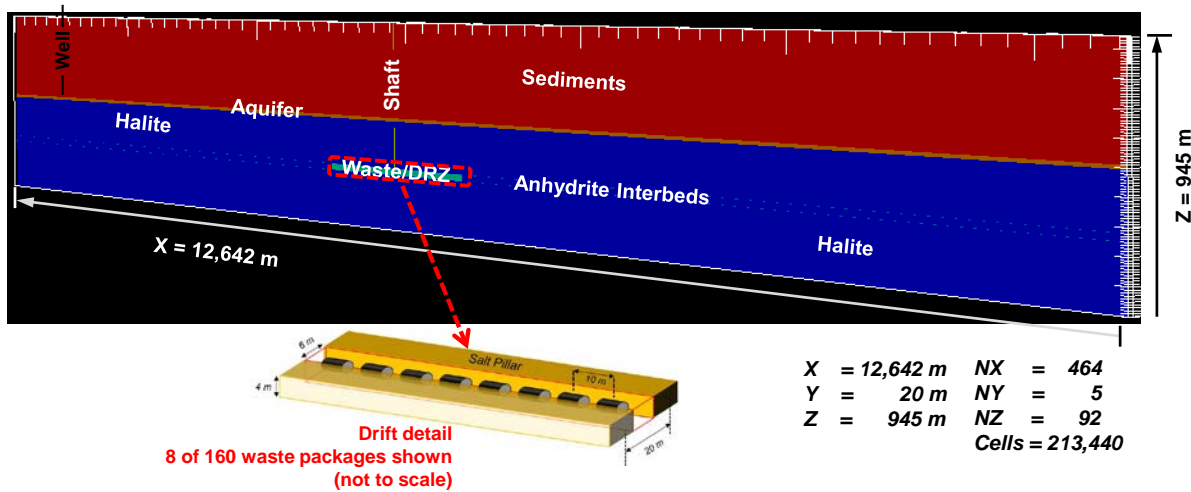

Fig. 5. PFLOTRAN model domain and blow-up of drift domain.

The "deterministic" or "best estimate" properties of the reference case (TABLE II) result in primarily diffusive/dispersive radionuclide transport (i.e., a low system Peclet number, N_{Pe}) through the halite and anhydrite regions, as indicated in TABLE III—assuming $N_{Pe} = 10$ as the division between predominantly diffusive/dispersive transport and advective transport [30, Fig. 5-14]. The Peclet number in each formation, resulting from the combination of molecular diffusion and kinematic dispersion, is defined as

$$N_{Pe} = \frac{uL_{sys}}{D_{eff} + \alpha_L u}$$
Eq. (4-2)

where $D_{eff} = \phi\tau D_{w,}$ is the effective diffusion coefficient (from TABLE II), α_L is the longitudinal dispersivity, u is the Darcy velocity, and L_{sys} is the system length, taken to be 5000 m, i.e., the distance from the edge of the repository to the withdrawal well.

TABLE III. System Peclet number, N_{Pe}, in the various regions.

Region	Darcy velocity, u (m/s)[a]	Effective Diffusion Coefficent, D_{eff} (m²/s)	Longitudinal Dispersivity (m)	Longitudinal dispersion coefficient, $D_L = \alpha_L u$ (m²/s)	Peclet Number, N_{Pe}
Halite	3.17×10^{-19}	4.19×10^{-13}	50.0	1.585×10^{-17}	0.0038
Interbed (anhydrite)	1.90×10^{-15}	5.57×10^{-12}	50.0	9.5×10^{-14}	1.7
Aquifer	1.58×10^{-9}	1.83×10^{-10}	50.0	7.9×10^{-8}	98
Sediments	1.58×10^{-11}	2.67×10^{-10}	50.0	7.9×10^{-10}	75

[a] from PFLOTRAN simulations

Radionuclide transport includes the effects of sorption and decay/ingrowth and, because ^{129}I is non-sorbing in the deterministic case ($K_d = 0$ ml/g) with no solubility limit and a long half-life, it is expected to be the most consequential radionuclide to reach the biosphere. Because of its instant release fraction, ^{129}I concentration is high in the repository region at early times compared to other radionuclides. Thus, it can be used to reveal details of the domain discretization, showing 160 emplaced waste packages in two opposing repository drifts—one drift on each side of the central hallway (Fig. 8). Typical PA models simulate a single waste package or a stylized "lumped" waste package. However, with the HPC-enhanced PA model capability, simulations can include a detailed representation of individual waste packages.
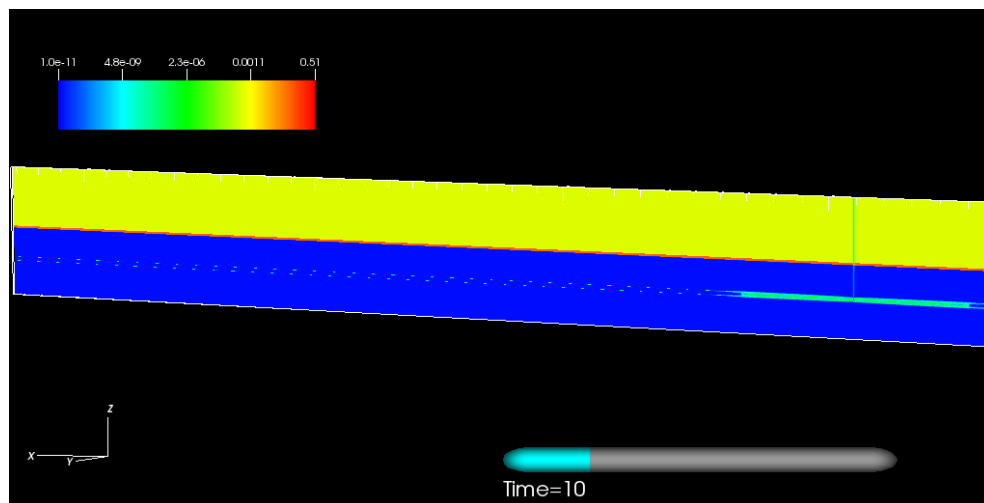

Fig. 6. Fluid velocity magnitude field (m/yr) for the deterministic isothermal generic salt repository domain.

8

Spatial profiles of [129]I concentration (reported as molality or mol/kg water) in the simulation domain are shown at various times in Fig. 9. The instant release (or "gap") fraction of [129]I, as well as [129]I released during waste form degradation, produces a high dissolved concentration at early times (e.g., 1000 years) in the waste-package and backfill regions (Fig. 9a), which subsequently diffuses into the DRZ and halite (Fig. 9b). At about 50,000 years, the [129]I from the waste form reaches and begins to travel through the aquifer (Fig. 9c), via upward transport through the shaft seal region. At 200,000 years, [129]I has been transported by advection down the length of both the aquifer and overburden sediments and is diffusing upward through the sediments (Fig. 9d). The importance of advective transport in the sediments (see TABLE III) is apparent from the shape of the concentration profile in Fig. 9d, which shows limited [129]I transport upstream of the shaft in either the aquifer or sediments.
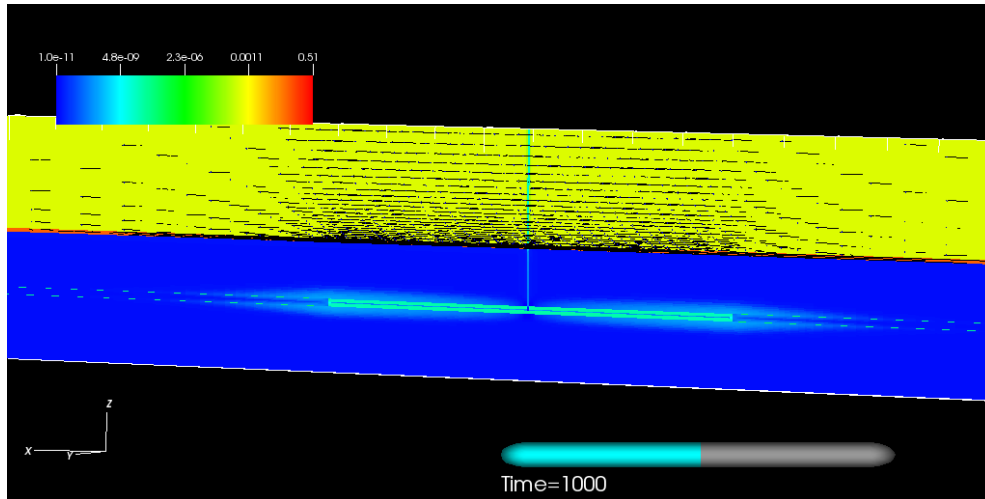

Fig. 7. Fluid velocity vector and magnitude field (m/yr) at 1000 years for the deterministic isothermal generic salt repository domain.
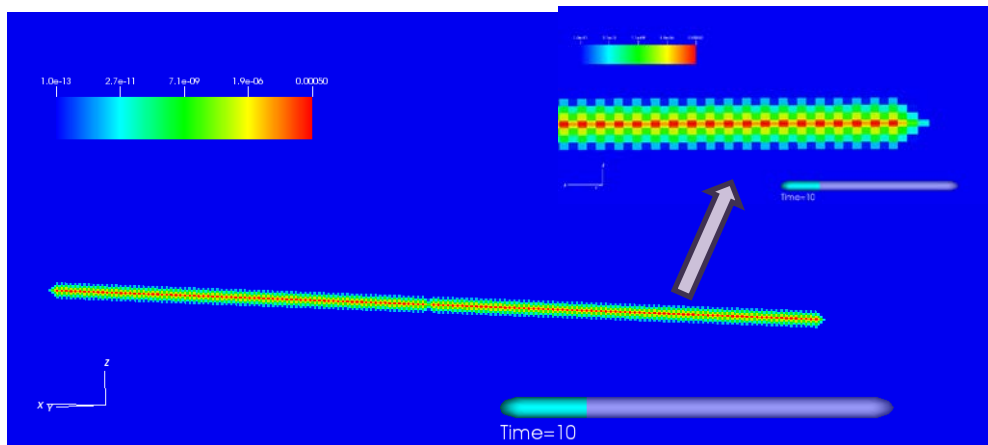

Fig. 8. [129]I dissolved concentration at 10 years, show waste package and drift detail.

The transport behavior of [129]I in Fig. 9 is a result of the assumed material properties in the various regions and may or may not occur at a potential repository site, depending on the measured properties. Its main purpose here is to demonstrate the capabilities of the enhanced PA model. Also, the indicated [129]I concentrations in Fig. 9 are conservatively high because the lateral boundary conditions in the *y*-direction (i.e., at the sides of the 20-m-wide, 3-D slice) are zero-gradient, no-flow. This prevents [129]I from leaving the system in the lateral direction. This would only be true of a repository with an "infinite" number of

parallel drifts and, thus, does not account for dilution from lateral mass loss, thereby biasing the results towards higher than expected concentrations in the aquifer and overburden. However, the purpose of these simulations is more of a demonstration of the capabilities of the GDSA framework, rather than as a rigorous investigation of the behavior of actual bedded salt repository system.
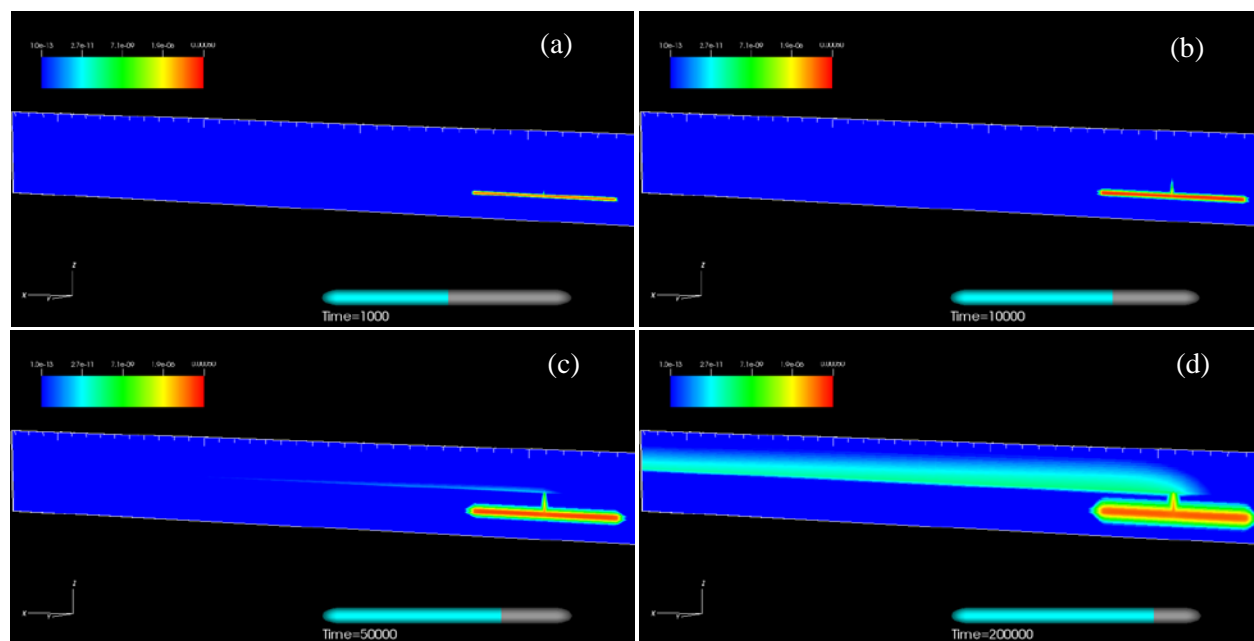

Fig. 9. ^{129}I dissolved concentration at specified times for the deterministic isothermal generic salt repository simulation: (a) 1,000 years, (b) 10,000 years, (c) 50,000 years, and (d) 200,000 years.

Probabilistic Isothermal Simulation Results

Probabilistic isothermal simulations of the salt repository demonstration problem were carried out to test the capabilities of the GDSA framework. Fifty realizations were run, with parameter sampling (using Latin Hypercube Sampling (LHS)) and sensitivity analyses performed using DAKOTA. The ten parameters selected for sampling are shown in TABLE IV.

TABLE IV. Salt repository reference case probabilistic properties.

Model Parameter	Deterministic Value	Probability Range	Distribution Type
Waste form degradation rate constant (mol/m^2/s)	4.8×10^{-8}	$1.00 \times 10^{-10} - 1.00 \times 10^{-7}$	Log uniform
^{129}I K_d^P (ml/g)	0.0	$9.28 \times 10^{-7} - 7.84 \times 10^{-3}$	Log uniform
^{237}Np K_d^P (ml/g)	5.5	$1.0 - 10.0$	Log uniform
Waste Package Porosity	0.30	$0.05 - 0.50$	Uniform
Backfill Porosity	0.113	$0.010 - 0.200$	Uniform
Shaft Porosity	0.113	$0.010 - 0.200$	Uniform
DRZ Porosity	0.0129	$0.0010 - 0.1000$	Uniform
Halite Porosity	0.0182	$0.0010 - 0.0519$	Uniform[a]
Anhydrite Interbed Permeability (m^2)	1.26×10^{-19}	$1.00 \times 10^{-21} - 1.00 \times 10^{-17}$	Log uniform[b]
Aquifer Permeability (m^2)	1.00×10^{-13}	$1.00 \times 10^{-14} - 1.00 \times 10^{-12}$	Log uniform

[a] The uniform distribution is a simplification of the cumulative distribution reported by Freeze et al. [13, Section 3.2.3.2].
[b] The log uniform distribution is a simplification of the Student-t distribution reported by Freeze et al. [13, Section 3.2.3.3].

Probabilistic results were output at ten different observation points as indicated in Fig. 10. The primary analyzed results at these observation points are time histories of [129]I dissolved concentrations for the 50 realizations of the probabilistic parameter sampling. These 50 time histories or "horsetail" plots are then post-processed with DAKOTA subroutines to provide plots of partial rank correlation coefficients (PRCCs) indicating the strength of dependency (effectively the derivative, or "local" sensitivity) of the variation in [129]I concentration versus variation in each sampled parameter. The [129]I concentrations used in the PRCC plots is the set of 50 maximum concentrations over the entire 1,000,000-year time span. Multi-realization plots of [129]I concentration (molal) are provided in Fig. 11 for nine of the observation points. PRCC bar charts are provided in Fig. 12 for four of these observation points. The PRCC bar charts all show similar dependencies of [129]I concentration on input parameter variation, except for an important difference related to shaft seal porosity for the "halite-near" point (as well as the "anhydrite-near" point, which is not shown here—see [15]). This is because [129]I reaches the anhydrite-near and halite-near observation points by a different pathway than [129]I for the other seven observation points. The pathway of [129]I transport to these two locations is strictly via upward diffusion from the repository zone to these points. No advective transport is involved. On the other hand, for the other seven observation points (aquifer-near, sediments-near, anhydrite-midx, halite-midx, aquifer-midx, sediments-midx, and aquifer monitor well) the [129]I transport pathway is via diffusion upward through the shaft seal region, followed by advectively dominated transport through the aquifer and sediments.
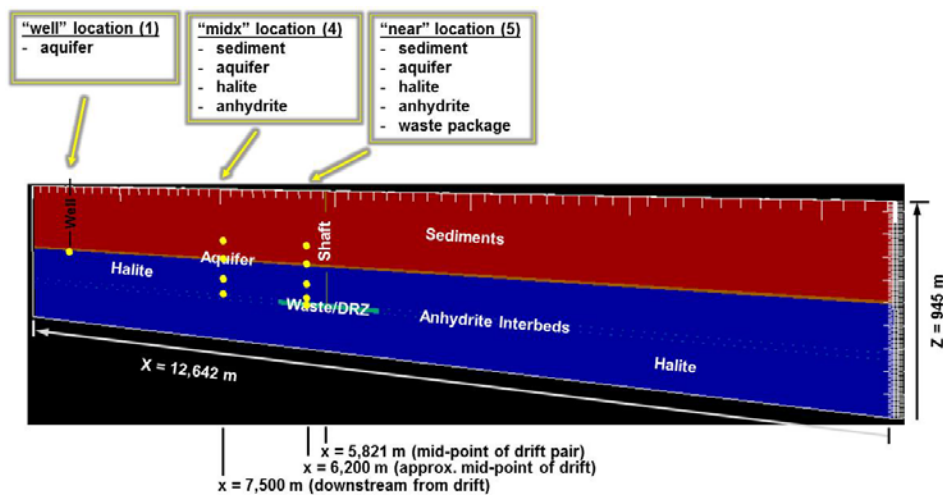

Fig. 10. Location of observation points for sensitivity analyses for the probabilistic isothermal generic salt repository simulation.

[129]I concentration variations at the anhydrite-near and halite-near observation points share strong dependencies on two of the same varied input parameters, with both points showing a strong positive correlation to the waste-form degradation rate and a strong negative correlation to the DRZ porosity. The positive dependence on the waste-form degradation rate is because this rate strongly influences the source concentration that drives the diffusion gradient toward the observation point (i.e., the concentration in the waste-package/waste-form cell, which is the upstream boundary condition for diffusive transport). The strong negative correlation to DRZ porosity is based on the same effect—i.e., the influence of source cell concentration. In particular, the greater the DRZ porosity (recall that the DRZ is directly adjacent to the repository zone) the faster the transport away from the source cells and, thus, the lower the concentration in the upstream source cell at long times. This lower source concentration then causes a lower concentration at the observation point because of the lower diffusion gradient from source to observation point. The halite-near location also has a strong negative dependence on the [129]I K_d. This is because of the long diffusive transport time and associated diffusive spreading of the [129]I wave front. This type of dependency on [129]I K_d is also shared with two other observation points, the anhydrite-midx (Fig. 12) and

halite-midx points, which have a transport pathway that is also highly dependent on diffusion. In particular, as noted below, [129]I reaches these two points via relatively fast transport along the aquifer and then slow downward diffusion.
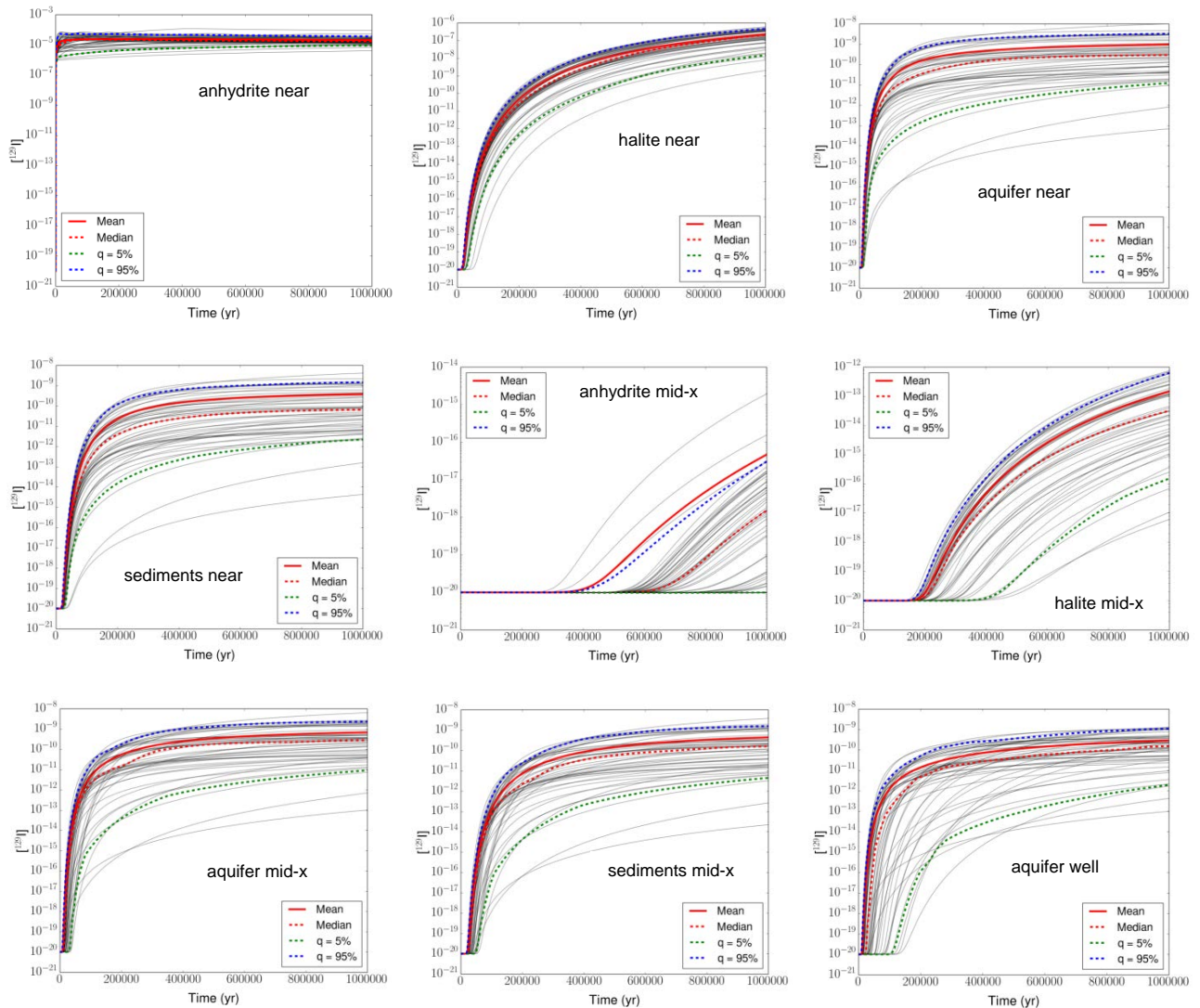

Fig. 11. Multi-realization time histories of [129]I dissolved concentration at various observation points for the probabilistic isothermal generic salt repository simulation.

The other seven observation points (aquifer-near, sediments-near, anhydrite-midx, halite-midx, aquifer-midx, sediments-midx, and aquifer monitor well) all show mostly similar PRCC behavior because they all are influenced by the same transport behavior, which is diffusion upward through the shaft seal region, followed by advectively dominated transport through the aquifer and sediments. This causes all seven points to exhibit a strong positive correlation to shaft seal porosity, since the rate of [129]I mass transfer to the aquifer is higher when the effective diffusion coefficient in the shaft region, $(D_{eff})_{shaft} = (\phi\tau)_{shaft}D_w$, is higher. Even the anhydrite-midx and halite-midx show this type of dependency on shaft seal porosity, although the actual magnitudes of their [129]I concentrations are very low (Fig. 11). In other words, the [129]I that reaches these observation points is by diffusive transport up the shaft seal, followed by relatively fast advection through the aquifer, and then slow diffusion downward from the aquifer to these points. The negative correlation of [129]I concentration with aquifer permeability for these seven observation points is

further evidence of the importance of advective transport through the aquifer, i.e., the higher the aquifer permeability, the greater the fluid flow rate, which implies a greater dilution of the [129]I concentration.
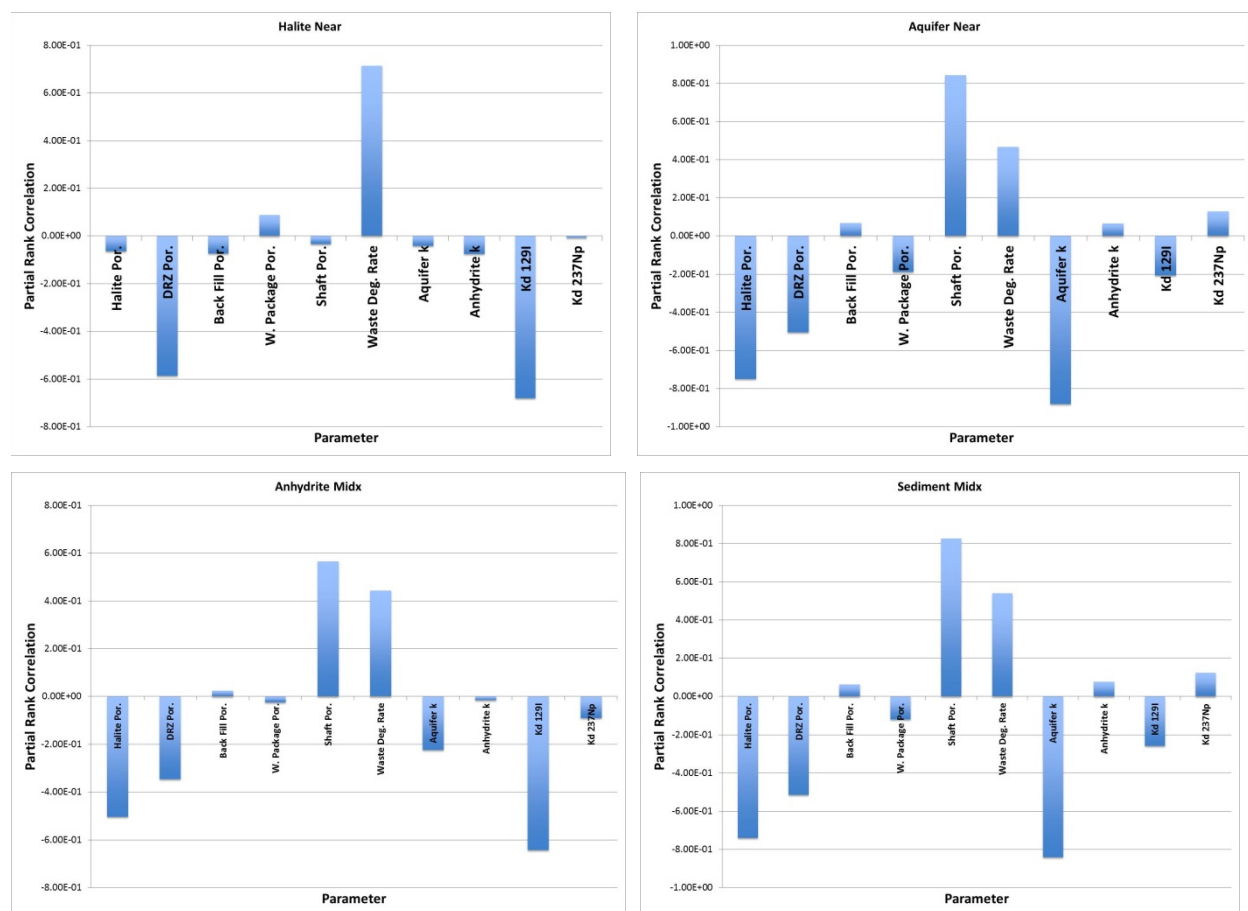

Fig. 12. Partial rank correlation coefficients for [129]I dissolved concentration versus sampled parameters for the probabilistic isothermal generic salt repository simulation for four observation points.

Deterministic Thermal Simulation Results

The salt repository *thermal* simulations were run using PFLOTRAN "General" option, which models multiphase air-water flow combined with the thermal energy equation [31]. Thermal properties of the various materials are given in TABLE II and the SNF source-term decay heat is from Carter et al. [25] for 60 GWd/MT PWR SNF.

The fluid velocity magnitude (in m/yr) and vector fields in all regions of the simulation domain (resulting from the applied hydraulic gradient of 0.0013) are shown in Figs. 13 and 14. Figure 13 shows Darcy velocity magnitude at 10 years for most of the simulated domain, while Fig. 14 shows velocity vectors at 10 years for a portion of the domain closer to the repository region, along with color profiles of the temperature field on a scale of 20°C to 230°C. In comparing Fig. 13 to the isothermal Darcy velocity magnitude field in Fig. 6, the primary difference is the halo of increased velocity magnitude surrounding the repository region in Fig. 13. The cause of this is made clear from Fig. 14, which indicates a strong component of fluid flux flowing away from the repository region, due to thermal expansion of the fluid. Fluid velocity direction and temperature fields are shown at other times in Fig. 15. The primary observation from the results in Fig. 15 comes from parts b, c, and d, the velocity vectors and temperatures at 1000 years, 10,000 years, and 50,000 years, respectively. These plots show the development of

buoyancy-driven fluid convection cells in the combined aquifer/sediments region over the first 10,000 years. Dissipation of the heat decay pulse lowers the temperature at the base of the aquifer enough (to a little below 35°C) such that by 50,000 years the Rayleigh number [32, 33, 34] is reduced to below the critical value for buoyancy-driven convection, which is clear from the velocity vectors in Fig. 15d.

When spatial profiles of [129]I concentration (reported as molality or mol/kg water) for the thermal simulation are compared at the same times with the isothermal simulation (Fig. 9), the thermal expansion of the fluid at early times causes a greater flux of [129]I transported laterally from the repository (upstream and downstream in the *x*-direction) in the thermal simulation (e.g. see Fig. 16). However, later [129]I concentration plots for *t* > 50,000 years (not shown, but see [15]) indicate little effect of the heat pulse in either the repository region or in the aquifer/sediments region. This is because the [129]I takes about 50,000 years to diffuse through the shaft seal region into the aquifer and sediments, which is beyond the time when thermal convection cells are present (see Fig. 15d). Thus, [129]I transport in the aquifer and sediments is not enhanced by these convection cells. Other conclusions about [129]I transport for this thermal simulation are the same as those discussed above for the isothermal simulation.
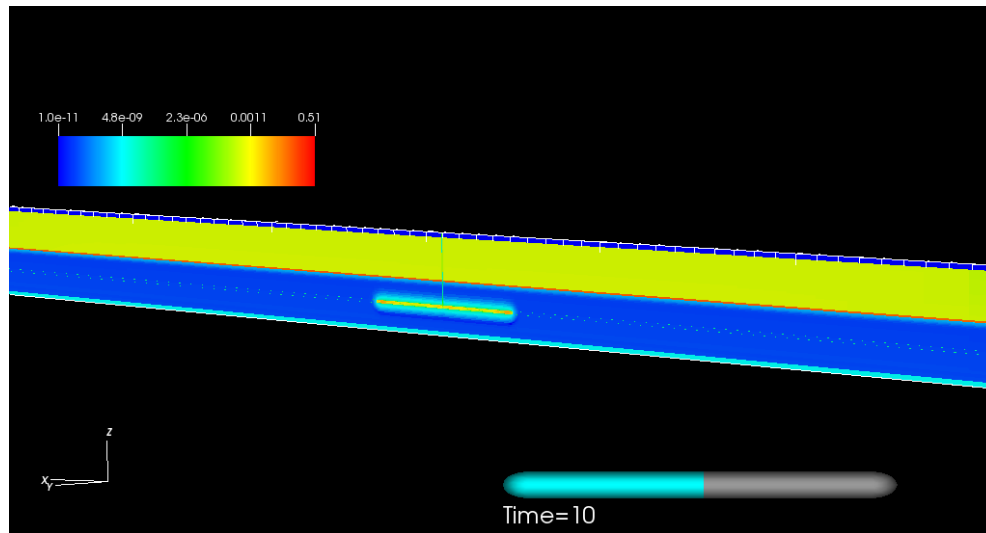

Fig. 13. Fluid velocity magnitude field (m/yr) for the deterministic *thermal* generic salt repository domain.
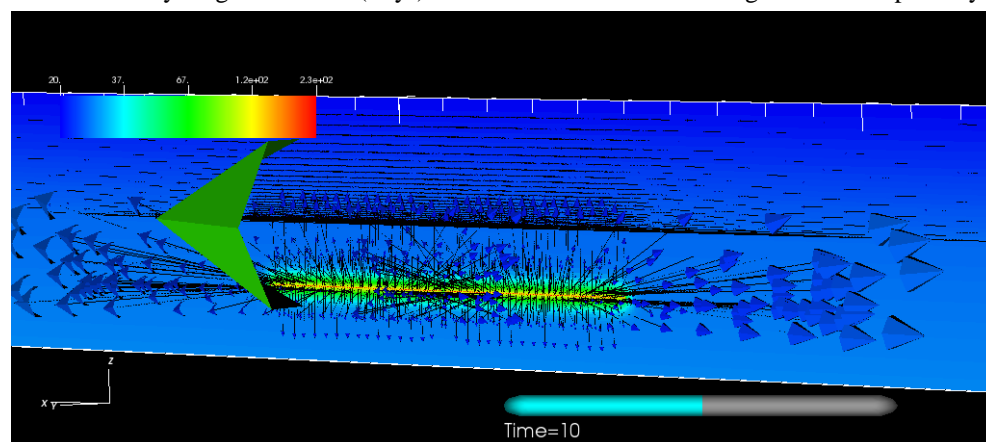

Fig. 14. Fluid velocity vector field (m/yr) and temperature field (on a scale of 20°C (blue) to 230°C (red)) at 10 years after repository closure for the deterministic *thermal* generic salt repository domain.
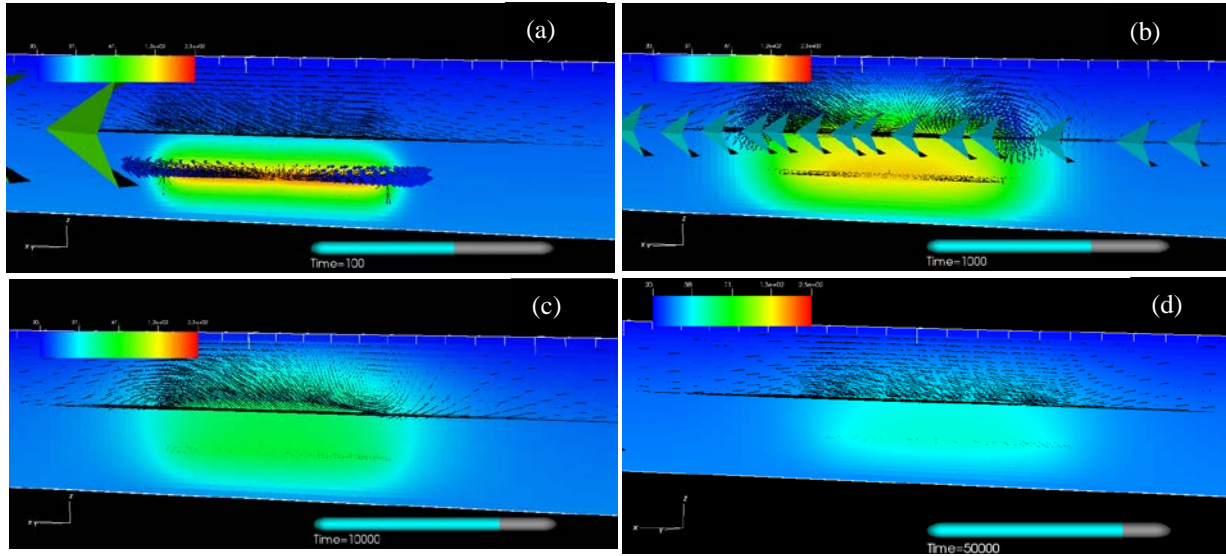
14

Fig. 15. Fluid velocity vector field (m/yr) and temperature field (on a scale of 20°C (blue) to 230°C (red)) at various times for the deterministic *thermal* generic salt repository domain: (a) 100 years, (b) 1000 years, (c) 10,000 years, and (d) 50,000 years.
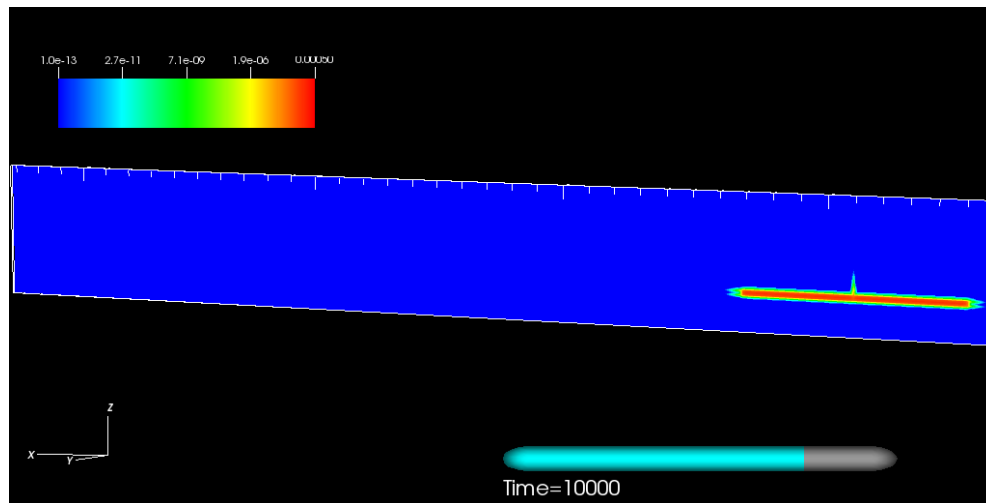

Fig. 16. [129]I dissolved concentration at 10,000 years for the deterministic *thermal* generic salt repository simulation.

Probabilistic Thermal Simulation Results

Probabilistic thermal simulations of the salt repository demonstration problem were carried out to test the coupled TH process capabilities of the GDSA framework. Fifty realizations were run, with parameter sampling (using Latin Hypercube Sampling (LHS)) and sensitivity analyses performed using DAKOTA. The ten parameters selected for sampling are shown above in TABLE IV. Differences in the multi-realization breakthrough curves of [129]I concentration (molal) between the thermal simulations and isothermal simulations are almost negligible because of the small effect of the thermal pulse on radionuclide transport, as previously discussed with regard to the deterministic thermal case. The only difference with much importance is for the "Anhydrite Mid-x" observation point where about 6 of the 50 realizations show nearly immediate breakthrough in the thermal case (Fig. 17a) but quite delayed breakthrough in the isothermal case (Fig. 11). This can be explained by examining the early-time fluid

15

flux vectors for the deterministic thermal case (Figs. 14 and 15a), which show the high early advective flux around the repository due to thermal expansion of the fluid. For some of the random samples of the anhydrite permeability distribution near the upper end of its range (TABLE IV), the advective flux in the anhydrite beds is high enough at early times (due to the thermal driving force) to cause rapid transport of the fast release fraction of ^{129}I to the "Anhydrite Mid-x" location. At least three of these high permeability samples are also noticeable in Fig. 11 as the three earliest breakthrough curves for the "Anhydrite Mid-x" location. This difference in three realizations does not result in any noticeable differences for the PRCC analysis (Fig. 17b).
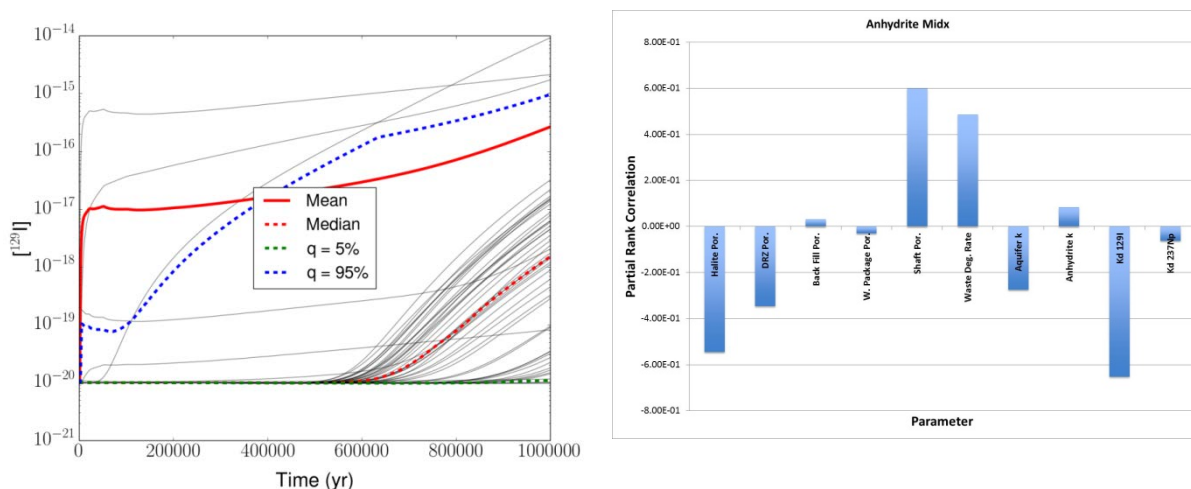

Fig 17. (a) Multi-realization time history of ^{129}I dissolved concentration and (b) partial rank correlation coefficients for ^{129}I dissolved concentration versus sampled parameters, and at the "anhydrite mid-x" observation point for the probabilistic *thermal* generic salt repository simulation.

SUMMARY AND CONCLUSIONS

This paper describes advances in performance assessment modeling of deep geologic repositories facilitated by a massively parallel, high-performance computing (HPC) environment. Our new Generic Disposal System Analysis (GDSA) Framework utilizes the massively parallel PFLOTRAN multi-physics code to simulate repository performance in the presence of coupled thermal-hydrologic-chemical processes, linked to DAKOTA, an HPC uncertainty sampling and propagation code that provides nested parallelism for multi-realization performance assessment and sensitivity analysis. The application of an HPC performance assessment framework is a significant advancement in PA modeling capability, allowing multi-physics couplings to be represented directly, rather than through simplified abstractions. This enhanced performance assessment (PA) modeling capability is demonstrated with deterministic and probabilistic simulations of a generic repository for SNF and HLW in bedded salt host rock, by comparisons of repository performance between a case with heat-generating waste ("thermal" case) and a case without heat generation ("isothermal" case). The simulation results provide preliminary insights into the effect of multi-physics processes and thermal-hydrologic coupling on the long-term behavior of a reference-case salt repository, but require additional refinement before being used as a definitive guide for future R&D. These preliminary results indicate that the effect of heat on radionuclide transport to the biosphere is likely not significant in a bedded salt repository, if only TH couplings are considered. However, the impact of THC, THM, and THMC coupling has not yet been investigated for the salt reference case and may have important effects on transport pathways and behavior for the nominal scenario. Also, disturbed scenarios still require investigation with the GDSA Framework.

REFERENCES

1. Sevougian, S. D. and R. J. MacKinnon 2014. "A Decision Methodology for Prioritizing R&D Supporting Geologic Disposal of SNF/HLW in Salt – 14030," in *Proceedings of the WM2014 Conference*, March 2 – 6, 2014, Phoenix, Arizona USA.

2. Freeze, G., M. Voegele, P. Vaughn, J. Prouty, W.M. Nutt, E. Hardin, and S.D. Sevougian 2013b. *Generic Deep Geologic Disposal Safety Case.* FCRD-UFD-2012-000146 Rev. 1, SAND2013-0974P. Sandia National Laboratories, Albuquerque, NM.

3. Sevougian, S. D., R. J. MacKinnon, C. D. Leigh, and F. D. Hansen 2013a. "A Safety Case Approach for Deep Geologic Disposal of DOE HLW and DOE SNF in Bedded Salt – 13350," in *Proceedings of the WM2013 Conference*, February 24 – 28, 2013, Phoenix, Arizona USA.

4. Freeze, G. and P. Vaughn 2012. *Development of an Advanced Performance Assessment Modeling Capability for Geologic Disposal of Nuclear Waste: Methodology and Requirements.* SAND2012-10208. Sandia National Laboratories, Albuquerque, NM.

5. Sevougian, S. D., G. Freeze, M. Gross, J. Wolf, J. Mönig, and D. Buhmann 2014a. "Generic Salt FEPs Catalogue – Volume I," Rev. 0, March 31, 2014, Carlsbad, NM: Sandia National Laboratories, Waste Isolation Pilot Plant (WIPP) Records Center, Sandia Level Three Milestone: No. INT-14-01.

6. Sevougian, S.D., G.A. Freeze, M.B. Gross, J. Lee, C.D. Leigh, P. Mariner, R.J. MacKinnon, and P. Vaughn 2012. *TSPA Model Development and Sensitivity Analysis of Processes Affecting Performance of a Salt Repository for Disposal of Heat-Generating Nuclear Waste.* FCRD-UFD-2012-000320 Rev. 0, U.S. Department of Energy, Office of Used Nuclear Fuel Disposition, Washington, DC.

7. Freeze, G., S.D. Sevougian, and M. Gross 2013c. *Safety Framework for Disposal of Heat-Generating Waste in Salt: Features, Events, and Processes (FEPs) Classification.* FCRD-UFD-2013-000191. SAND2013-5220P. Sandia National Laboratories, Albuquerque, NM.

8. Freeze, G., S. D. Sevougian, C. Leigh, M. Gross, J. Wolf, J. Mönig, and D. Buhmann 2014a. "A New Approach for Feature, Event, and Process (FEP) Analysis of UNF/HLW Disposal – 14314," in *Proceedings of the WM2014 Conference*, March 2 – 6, 2014, Phoenix, Arizona USA.

9. Adams, B.M., M.S. Ebeida, M.S. Eldred, J.D. Jakeman, L.P. Swiler, W.J. Bohnhoff, K.R. Dalbey, J.P. Eddy, K.T. Hu, D.M. Vigil, L.E. Baumann, and P.D. Hough 2013. *Dakota, a Multilevel Parallel Object-Oriented Framework for Design Optimization, Parameter Estimation, Uncertainty Quantification, and Sensitivity Analysis, Version 5.3.1+ Theory Manual.* SAND2011-9106, Updated May 22, 2013. Sandia National Laboratories, Albuquerque, NM. (http://dakota.sandia.gov/)

10. Hammond, G.E., P.C. Lichtner and R.T. Mills 2014. "Evaluating the Performance of Parallel Subsurface Simulators: An Illustrative Example with PFLORAN", *Water Resources Research*, 50, doi:10.1002/2012WR013483.

11. Balay S., J. Brown, K. Buschelman, V. Eijkhout, W.D. Gropp, D. Kaushik, M.G. Knepley, L. Curfman McInnes, B.F. Smith and H. Zhang 2013. *PETSc Users Manual*, ANL-95/11 – Revision 3.4, Argonne National Laboratory, Argonne IL.

12. Jerden J., K. E. Frey, J. M. Copple, and W. Ebert 2014. *ANL Mixed Potential Model For Used Fuel Degradation: Application to Argillite and Crystalline Rock Environments*, FCRD-UFD-2014-000490, U.S. Department of Energy, Office of Used Nuclear Fuel Disposition, Washington, DC, July 14, 2014.

13. Freeze, G., P. Gardner, P. Vaughn, S.D. Sevougian, P. Mariner, V. Mousseau, and G. Hammond 2013a. *Enhancements to Generic Disposal System Modeling Capabilities.* FCRD-UFD-2014-000062. SAND2013-10532P. Sandia National Laboratories, Albuquerque, NM.

14. Freeze, G., W. P. Gardner, P. Vaughn, S. D. Sevougian, P. Mariner, G. Hammond, and V. Mousseau 2014b. "Performance Assessment Modeling of a Generic UNF/HLW Repository in Salt – 14313," in *Proceedings of the WM2014 Conference*, March 2 – 6, 2014, Phoenix, Arizona USA.

15. Sevougian, S. D., G.A. Freeze, W.P. Gardner, G. E. Hammond, and P. Mariner 2014b. *Performance Assessment Modeling and Sensitivity Analyses of Generic Disposal System Concepts*. FCRD-UFD-2014-000320, SAND2014-17658. Sandia National Laboratories, Albuquerque, NM, September 12, 2014.

16. SKB (Svensk Kärnbränslehantering AB) 2010. *Data Report for the Safety Assessment SR-Site*. Technical Report TR-10-52. Swedish Nuclear Fuel and Waste Management Co., Stockholm, Sweden.

17. Kienzler, B., M. Altmaier, C. Bube, and V. Metz 2012. *Radionuclide Source Term for HLW Glass, Spent Nuclear Fuel, and Compacted Hulls and End Pieces (CSD-C Waste)*, KIT Scientific Publishing, Report-Nr. KIT-SR 7624, Karlsruher Institut für Technologie (KIT), Straße am Forum 2, D-76131 Karlsruhe, www.ksp.kit.edu

18. DOE (U.S. Department of Energy) 2009. *Title 40 CFR Part 191 Subparts B and C Compliance Recertification Application for the Waste Isolation Pilot Plant*. DOE/WIPP 09-3424. U.S. Department of Energy, Carlsbad Area Office, Carlsbad, NM, http://www.wipp.energy.gov/library/CRA/ 2009_CRA/CRA/Appendix_SOTERM/Appendix_SOTERM.htm

19. DOE (U.S. Department of Energy) 2008. *Yucca Mountain Repository License Application Safety Analysis Report.* DOE/RW-0573, Revision 1. U.S. Department of Energy, Washington, DC. (http://www.nrc.gov/waste/hlw-disposal/yucca-lic-app/yucca-lic-app-safety-report.html#1)

20. SNL 2008. *Total System Performance Assessment Model/Analysis for the License Application*, Volume 1, MDL-WIS-PA-000005 REV 00 ADD 01 ERD 4. Las Vegas, Nevada: Sandia National Laboratories. ACC: DOC.20080312.0001, DIRS 183478.

21. Sassani D. et al. 2012. *Integration of EBS Models with Generic Disposal System Models.* FCRD-UFD-2012-000277, SAND2012-7762P. Sandia National Laboratories, Albuquerque, NM, September 7, 2012.

22. Millington, R. J. 1959. "Gas Diffusion in Porous Media," *Science* **130**: 100-102.

23. Schwartz, F.W. and H. Zhang 2003. *Fundamentals of Ground Water*. New York: John Wiley & Sons, Inc.

24. Olivella S. 1995. *Nonisothermal Multiphase Flow of Brine and Gas Through Saline Media*, Doctoral Thesis, Technical University of Catalunya, Barcelona, Spain, June 1995.

25. Carter, J. T., A. J. Luptak, J. Gastelum, C. Stockman, and A. Miller 2012. *Fuel Cycle Potential Waste Inventory for Disposition*. FCRD-USED-2010-000031, Rev. 5. U.S. Department of Energy, Office of Used Nuclear Fuel Disposition, Washington, DC.

26. Freeze, R.A. and J.A. Cherry 1979. *Groundwater*, Prentice-Hall, Englewood Cliffs, NJ.

27. Hardin, E., T. Hadgu, D. Clayton, R. Howard, H. Greenberg, J. Blink, M. Sharma, M. Sutton, J. Carter, M. Dupont, and P. Rodwell 2012. *Repository Reference Disposal Concepts and Thermal Load Management Analysis.* FCRD-UFD-2012-000219 Rev. 2. U.S. Department of Energy, Office of Used Nuclear Fuel Disposition, Washington, DC.

28. Fox, B. 2008. *Parameter Summary Report for CRA-2009, Revision 0*, WIPP:1.2.5:PA:QA-L:547488, Sandia National Laboratories, Carlsbad, NM.

29. Lichtner, P. C., G. E. Hammond, C. Lu, S. Karra, G. Bisht, B. Andre, R. Mills, and J. Kumar 2014. *PFLOTRAN User Manual: A Massively Parallel Reactive Flow and Transport Model for Describing Surface and Subsurface Processes*, http://www.pflotran.org/docs/user_manual.pdf

30. Lake, Larry W. 1989. *Enhanced Oil Recovery*, Prentice-Hall, Englewood Cliffs, NJ 07632.

31. Lichtner, P. C. 2014. *PFLOTRAN: Technical Design Documentation for Two-Phase Air-Water System*, draft, May 7, 2014.

32. Beck, J. L. 1972. "Convection in a Box of Porous Material Saturated with Fluid," *The Physics of Fluids*, Vol. 15, No. 8, August 1972.

33. Nield, D. A. 1997. "Notes on Convection in a Porous Medium: (i) an Effective Rayleigh Number for an Anisotropic Layer, (ii) the Malkus Hypothesis and Wavenumber Selection," *Transport in Porous Media* **27**: 135–142, 1997.

34. Nield, D. A. and C. T. Simmons 2007. "A discussion on the effect of heterogeneity on the onset of convection in a porous medium," *Transp Porous Med* (2007) 68:413–421

ACKNOWLEDGEMENTS